TABLE III
PRECISION EVALUATION USING STEREO VISION

Calibration method	Linear	Nonlinear	Proposed
$\overline{\lvert\delta X_w\rvert}$ (μm)	39.7000	5.6711	6.0003
$\overline{\lvert\delta Y_w\rvert}$ (μm)	55.6575	18.1429	18.5753
$\overline{\lvert\delta Z_w\rvert}$ (μm)	29.3909	15.2511	15.8119
$\overline{\delta D_w}$ (μm)	82.6229	27.4295	28.0719
$\overline{\lvert\delta N_p\rvert}$	5.1279E-04	3.0102E-04	3.8576E-04
$\overline{\lvert\delta L\rvert}$ (μm)	53.1198	11.6246	10.9733

The measurements repeat 10 times, and the averages of the error measures are listed in Table III. As can be seen in Table III, the orientation errors of the planar features are all very small. The average absolute position error using the linear method is 82.62 μm, and the average location error of planar features is 53.12 μm. Using the proposed method, the average absolute position error is reduced to 28.07 μm, and the location error is less than 11.0 μm, which are comparable to those obtained using the nonlinear method.

VI. CONCLUSION

An automatic camera calibration scheme that utilizes a CMM and a novel camera calibration algorithm is presented for a multiple-sensor integrated coordinate measurement system. Distinct from other multiple-stage methods, the proposed camera calibration method requires neither particular initial guess procedure nor nonlinear minimization process. Synthetic and experimental tests have demonstrated that accurate camera calibration and precise coordinate measurements can be obtained using the proposed calibration scheme. With high-precision calibration targets generated automatically using CMM and the proposed camera calibration algorithm, a fully automated and accurate camera calibration process can be performed for a multiple-sensor integrated system.

REFERENCES

[1] Y. I. Abdel-Aziz and H. M. Karara, "Direct linear transformation into object space coordinates in close-range photogrammetry," in *Proc. Symp. on Close-Range Photogrammetry*, Urbana, IL, Jan. 1971, pp. 1–18.

[2] H. Bacakoglu and M. S. Kamel, "A three-step camera calibration method," *IEEE Trans. Instrum. Meas.*, vol. 46, pp. 1165–1172, 1997.

[3] C. Chatterjee, V. P. Roychowdhury, and E. K. P. Chong, "A nonlinear Gauss–Seidel algorithm for noncoplanar and coplanar camera calibration with convergence analysis," *Computer Vision and Image Understanding*, vol. 67, no. 1, pp. 58–80, 1997.

[4] J. Z. C. Lai, "On the sensitivity of camera calibration," *Image and Vision Computing*, vol. 11, pp. 656–664, 1993.

[5] R. K. Lenz and R. Y. Tsai, "Techniques for calibration of the scale factor and image center for high accuracy 3-D machine vision metrology," *IEEE Trans. Pattern Anal. Mach. Intell.*, vol. 10, pp. 713–720, 1988.

[6] American Society of Photogrammetry, *Manual of Photogrammetry*, 4th ed., 1980.

[7] R. B. Nelson, "Simplified calculation of eigenvector deviations," *AIAA J.*, vol. 14, pp. 1201–1205, 1976.

[8] T. S. Shen, "Multiple-sensor integration for rapid and high-precision coordinate metrology," Ph.D. dissertation, Dep. Mech. Eng., Ohio State Univ., Columbus, 2000.

[9] T. S. Shen, J. Huang, and C. H. Menq, "Multiple-sensor integration for rapid and high-precision coordinate metrology," *IEEE/ASME Trans. Mechatron.*, vol. 5, pp. 110–121, 2000.

[10] S. W. Shih, Y. P. Hung, and W. S. Lin, "Accurate linear technique for camera calibration considering lens distortion by solving an eigenvalue problem," *Opt. Eng.*, vol. 32, no. 1, pp. 138–149, 1993.

[11] R. Y. Tsai, "A versatile camera calibration technique for high-accuracy 3D machine vision metrology using off-the-shelf TV camera and lenses," *IEEE Trans. Robot. Automat.*, vol. RA-3, pp. 323–344, Aug. 1987.

[12] J. Weng, P. Cohen, and M. Herniou, "Camera calibration with distortion models and accuracy evaluation," *IEEE Trans. Pattern Anal. Mach. Intell.*, vol. 14, pp. 965–980, Oct. 1992.

A New Partitioned Approach to Image-Based Visual Servo Control

Peter I. Corke and Seth A. Hutchinson

***Abstract*—In image-based visual servo control, where control is effected with respect to the image, there is no direct control over the Cartesian velocities of the robot end effector. As a result, the robot executes trajectories that are desirable in the image, but which can be indirect and seemingly contorted in Cartesian space. In this paper, we introduce a new partitioned approach to visual servo control that overcomes this problem. In particular, we decouple the z-axis rotational and translational components of the control from the remaining degrees of freedom. Then, to guarantee that all features remain in the image throughout the entire trajectory, we incorporate a potential function that repels feature points from the boundary of the image plane. We illustrate our new control scheme with a variety of results.**

***Index Terms*—Image-based visual servo, potential field, visual servo.**

I. INTRODUCTION

In image-based visual servo (IBVS) control, an error signal is measured in the image and mapped directly to actuator commands (see, e.g., [1] and [2]). This in contrast to positition-based visual servo (PBVS) systems in which extracted features are used to compute a (partial) 3-D reconstruction of the environment or of the motion of a target object in the environment [3]. An error is then computed in the task space and it is this error that is used by the control system.

IBVS approaches have seen increasing popularity, largely due to the shortcomings of PBVS systems. With PBVS, any errors in calibration of the vision system will lead to errors in the 3-D reconstruction and subsequently to errors during task execution. In addition, since the control law for PBVS is defined in terms of the 3-D workspace, there is no mechanism by which the image is directly regulated. Thus, it is possible that objects of interest (including features that are being used by the visual servo system) can exit the camera's field of view.

However, there are problems associated with IBVS systems. For an IBVS system, the control law involves the mapping between image space velocities and velocities in the robot's workspace. This mapping is encoded in the image Jacobian (which will be briefly reviewed in Section II). Singularities or poor conditioning in this Jacobian (which occur as a function of the relative position and motion of the camera and the object under observation) lead to control problems. Secondly, since control is effected with respect to the image, there is no direct control

Manuscript received November 29, 2000. This paper was recommended for publication by Associate Editor P. Allen and Editor A. De Luca upon evaluation of the reviewers' comments.

P. I. Corke is with CSIRO Manufacturing Science & Technology, Pinjarra Hills, Australia 4069.

S. A. Hutchinson is with the Beckman Institute for Advanced Technology, University of Illinois at Urbana-Champaign, Urbana, IL 61801 USA.

Publisher Item Identifier S 1042-296X(01)08447-6.

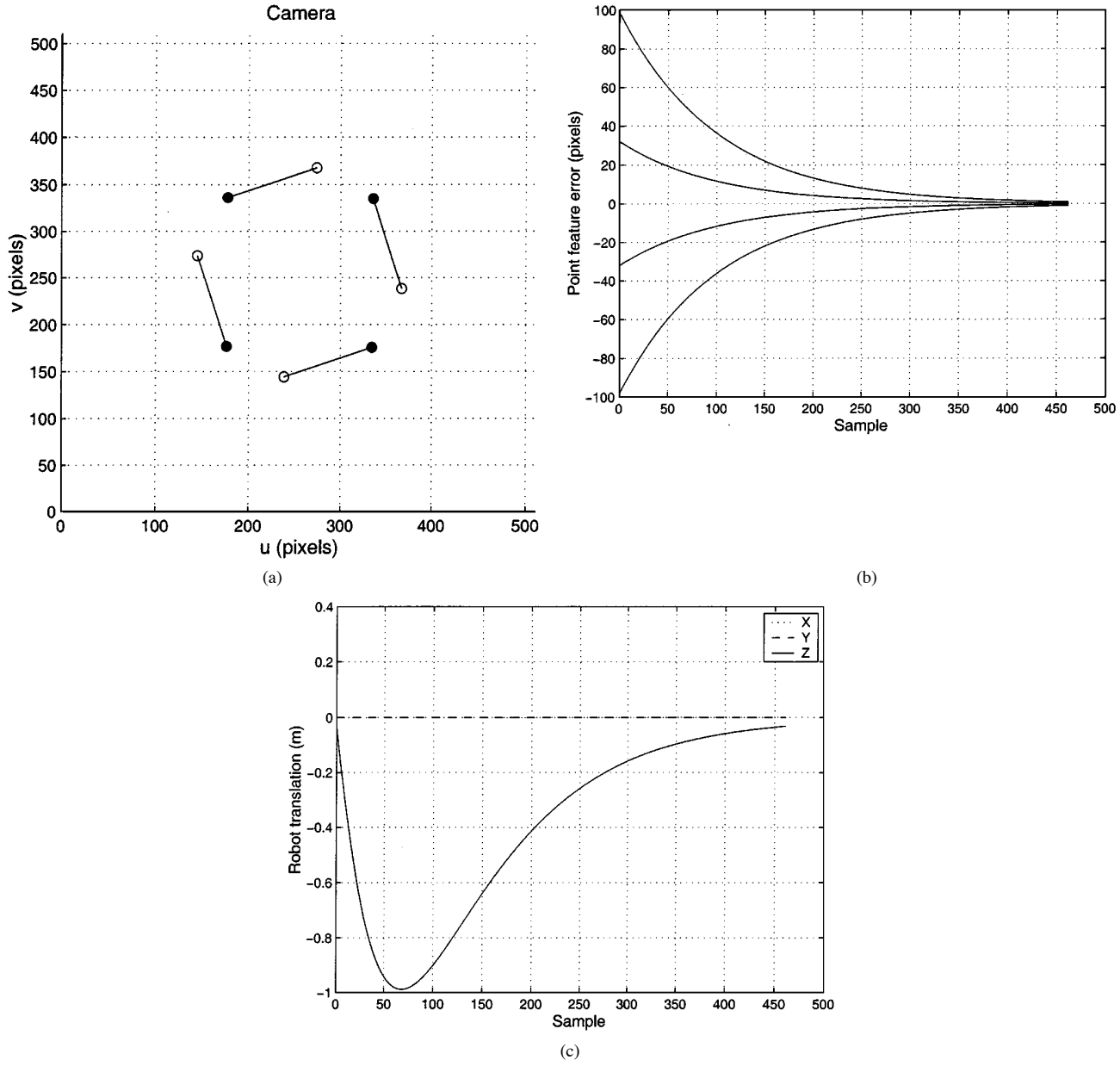

Fig. 1. IBVS for pure target rotation (0.3 rad). (a) Image-plane feature motion (initial location is o, desired location is •). (b) Feature error trajectory. (c) Cartesian translation trajectory.

over the Cartesian velocities of the robot end effector. Thus, trajectories that the robot executes, while producing image trajectories that are visually appealing, can appear quite contorted in the Cartesian space. In Section III, we discuss a recent example due to Chaumette [4] in which IBVS moves the camera along an extremely suboptimal Cartesian trajectory, while driving it toward a singularity in the image Jacobian.

These performance problems with IBVS systems have led to the recent introduction of several hybrid methods [5]–[7]. Hybrid methods use IBVS to control certain degrees of freedom while using other techniques to control the remaining degrees of freedom. In Section IV, we describe a number of these hybrid approaches and how they address specific performance issues.

In Sections V and VI, we present a new partitioned visual servo control scheme that overcomes a number of the performance problems faced by previous systems. The basic idea is to decouple the z-axis motions (including both the translational component and rotational component) from the other degrees of freedom and to derive separate controllers for these z-axis motions. Our new approach is computationally inexpensive and improves performance, particularly for tasks that require large Z-axis rotation (including the example of Chaumette [4]). We then incorporate techniques borrowed from the robot motion planning literature to guarantee that all features remain within the field of view.

Throughout the paper, we illustrate various concepts and methods with simulation results. We note here that in all simulations, the image features are the coordinates of the vertices of a unit square (1 m side length) in the XY plane intersecting the Z axis at $z = 8$ m. The camera uses a central projection model, with focal length $\lambda = 8$ mm, square pixels of side length 10 μm, and the principal point is (256, 256).

II. Traditional IBVS

In this section, we present a very brief review of image-based visual servo control. Let $r = (x, y, z)^T$ represent coordinates of the end-ef-

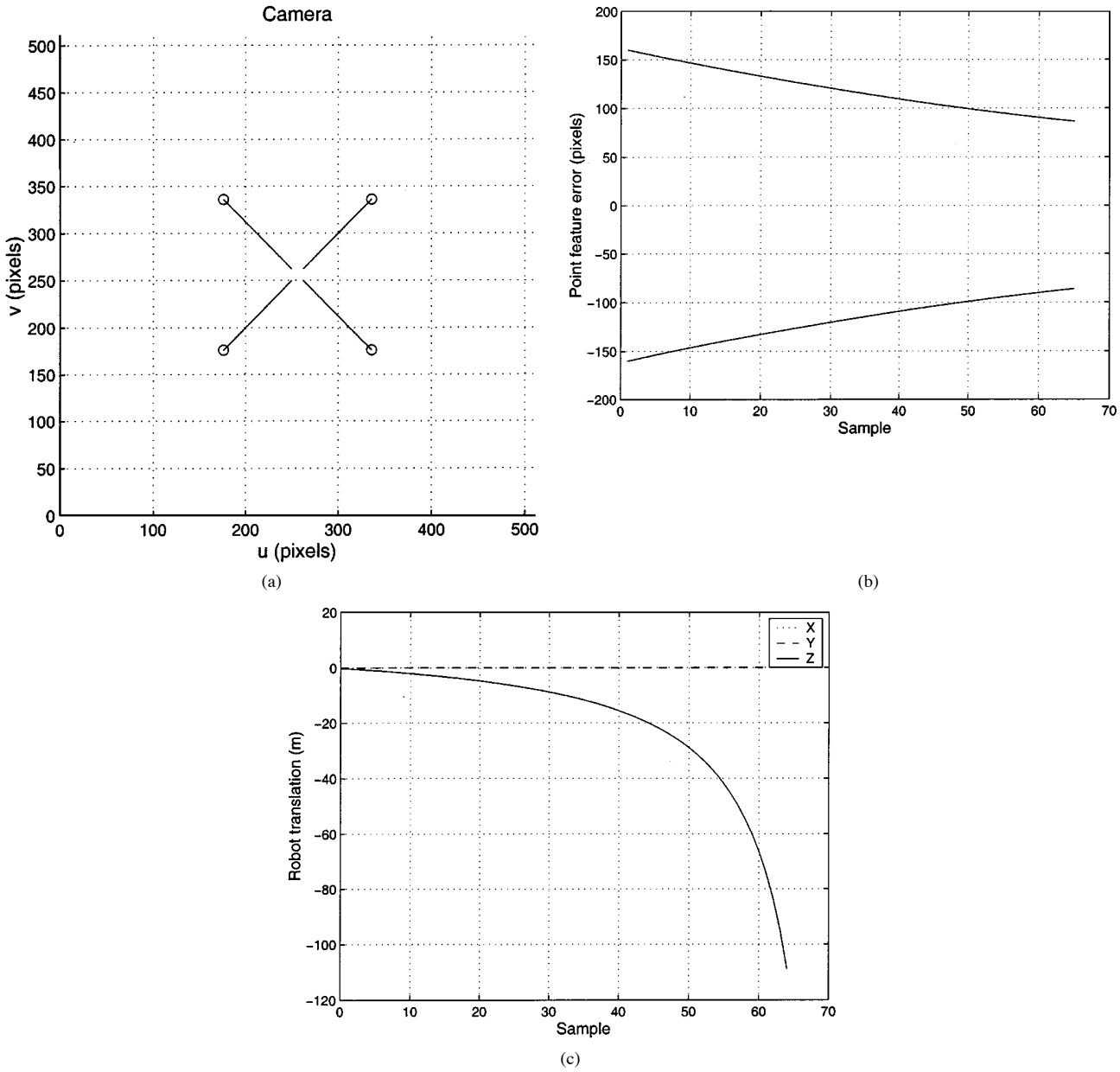

Fig. 2. Performance of classical IBVS with the Chaumette example. (a) Image-plane feature motion (initial location is o, desired location is •). (b) Feature error trajectory. (c) Cartesian translation trajectory.

fector and $\dot{r} = (T_x, T_y, T_z, \omega_x, \omega_y, \omega_z)^T$ represent the corresponding end-effector velocity, composed of a linear velocity $\mathbf{v} = (T_x, T_y, T_z)^T$ and angular velocity $\omega = (\omega_x, \omega_y, \omega_z)^T$. Let $f = (u, v)^T$ be the image-plane coordinates of a point in the image and $\dot{f} = (\dot{u}, \dot{v})^T$ the corresponding velocities. The image Jacobian relationship is given by

$$\dot{f} = J(f, r)\dot{r} \tag{1}$$

with

$$J = \begin{bmatrix} \frac{\lambda}{z} & 0 & \frac{-u}{z} & \frac{-uv}{\lambda} & \frac{\lambda^2+u^2}{\lambda} & -v \\ 0 & \frac{\lambda}{z} & \frac{-v}{z} & \frac{-\lambda^2-v^2}{\lambda} & \frac{uv}{\lambda} & u \end{bmatrix} \tag{2}$$

in which λ is the focal length for the camera. Derivations of this can be found in [8]. The image Jacobian was first introduced by Weiss *et al.* [1]. The most common image Jacobian is based on the motion of points in the image (e.g., [2], [9], [10]), but many other image features have been used in visual servo schemes.

The simplest approach to IBVS is to merely use (1) to construct the control law

$$\mathbf{u} = \Gamma J^{-1}(f, r)\dot{f} \tag{3}$$

in which $\dot{f}$ is the desired feature motion on the image plane, Γ is a gain matrix, and $\mathbf{u} = \dot{r}$ is the control input. If the image Jacobian is not square a generalized inverse, J^+, is used. Since (3) essentially represents a gradient descent on the feature error, when this control law is used, feature points move in straight lines to their goal positions. This can be seen in Fig. 1(a).

More sophisticated control schemes can be found in a variety of sources, including [11] where state space design techniques are used and [9] where the task function approach is used.

III. IBVS Suboptimal Cartesian Motions

A commonly mentioned criticism of IBVS is that the Cartesian paths often involve large camera motions, which are undesirable. Often the camera moves away from the target in a normal direction and then returns, a phenomenon we refer to as *camera retreat*. Such motion is not time optimal, requires large and possibly unachievable robot motion, and is a seemingly nonintuitive solution to the required image plane motion. Fig. 1 illustrates the problem. In Fig. 1(a), the feature points are seen to be driven on straight line trajectories to their goal positions, producing a large and unnecessary motion in the z direction, seen in Fig. 1(c).

In [4], Chaumette introduced an extreme version of this problem, which we refer to as the Chaumette Conundrum, illustrated in Fig. 2. Here, the desired camera pose corresponds to a pure rotation about the optic axis by π rad, i.e., the image feature point with initial coordinates (u, v) has the desired coordinates $(-u, -v)$. Control laws such as (3) drive the feature points in straight lines and in this case they are driven toward the origin, which corresponds to a singularity in the image Jacobian. The singularity arises because the feature points will reach the origin when the camera retreats to a distance of infinity and no motion can be observed. Thus, in the Chaumette Conundrum, we observe two performance problems acting synergistically: 1) the controller is driven toward a singular configuration and 2) this singular configuration is approached asymptotically and thus the system will servo forever without reaching the goal. We note that, as mentioned in [4], this problem cannot be detected by simply examining the image Jacboian, since the image Jacobian is well conditioned (at least initially). We use the term *IBVS failure* to refer to cases for which the system fails to achieve its goal.

At first it might seem that some rotational motion of the camera about its optic axis should be induced for the Chaumette Conundrum; however, this is not the case. The ω_z component of (3) is given by

$$\omega_z = (J^+)_6 \dot{f} \tag{4}$$

in which $(J^+)_6$ denotes the bottom row of the generalized inverse. In this particular case, even though $\dot{f} \neq 0$, the inner product is zero, i.e., the various contributions to rotational velocity cancel one another.

This camera retreat phenomenon can be explained in simple geometric terms, leading to a model that predicts the magnitude of the camera retreat motion. For the example of Fig. 1, a pure rotational motion of the camera would cause the points to follow an arc from point A to point B, as shown in Fig. 3. In order for the points to follow a straight line, as specified by (3), the scale must be changed so as to move the point from B to C. The required change in scale is given simply by the ratio of the distances OC and OB. The scale reduction attains its maximum value at $\theta = \alpha/2$ for which

$$\left(\frac{OC}{OB}\right)_{\max} = \cos\frac{\alpha}{2}. \tag{5}$$

In IBVS, the reduction in scale is achieved by moving the camera away from the target. The reduction in the apparent length of the line segment is inversely proportional to the distance that the camera retreats, and therefore

$$\frac{OC}{OB} = \frac{d_{\text{targ}}}{d} \tag{6}$$

in which d is the current distance to the target and d_{targ} is the desired target distance and assuming the camera is moving normal to the target. The maximum reduction is thus given by

$$d_{\max} = \frac{d_{\text{targ}}}{\cos\frac{\alpha}{2}}. \tag{7}$$

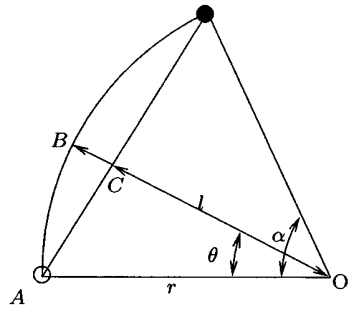

Fig. 3. Camera retreat model.

For the Chaumette Conundrum, in which $\alpha = \pi$, the model accurately predicts infinite camera retreat. The maximum camera retreat ratio observed in visual servo simulations and the simple model of (7) are compared in Fig. 4 and show close agreement.

There are a variety of possible solutions to this camera retreat problem. The requirement that points move in a straight line to their goal positions could be relaxed, giving rise to an image feature trajectory planning problem. The target depth, z, could be underestimated, causing the points to move in an arc instead of a straight line, reducing the magnitude of camera retreat [4], but this will still fail for the Chaumette Conundrum. The introduction of line segment features helps somewhat but Chaumette notes that such an approach is not guaranteed to solve the performance problems [4] and our own simulation results support this conclusion. Finally, the z-axis translational and rotational motions could be decoupled from the control law of (3) and separate controllers could be designed to enforce appropriate rotational and retreat motions. This latter approach leads to hybrid approaches that combine aspects of IBVS and PBVS systems. In Section IV, we describe several such approaches that have been recently introduced. Then, in Section V, we introduce our new partitioned method.

IV. Some Recent Hybrid Approaches

A number of authors [5]–[7] have recently addressed the problems above by proposing hybrid control architectures. In each of these approaches, (1) is decomposed into translational and rotational components

$$\dot{f} = J_v(u, v, z)\mathbf{v} + J_\omega(u, v)\omega \tag{8}$$

where $J_v(u, v, z)$ contains the first three columns of the image Jacobian and is a function of both the image coordinates of the point and its depth and $J_\omega(u, v)$ contains the last three columns of the image Jacobian and is a function of only the image coordinates of the point (i.e., it does not depend on depth).

Alternate techniques are used to compute the rotational [5], [6] or translational [7] velocity demand. Feature point coordinate error, $\dot{f}$, as in the traditional IBVS scheme and (8) is then used to determine the remaining component of the velocity. Yet another approach is to partion the axes according to dynamic performance [12].

The hybrid methods [5]–[7] all use the epipolar geometry to determine certain components of the camera motion while using an IBVS approach to determine the remaining component of the velocity. These methods rely on the online computation of the epipolar geometry of the camera [13], which amounts to computing a homography between two images. This homography is encapsulated in the fundamental matrix (for uncalibrated cameras) or essential matrix (for cameras with intrinsic parameters calibrated). The homography must then be decomposed to extract the rotational component and the problem of

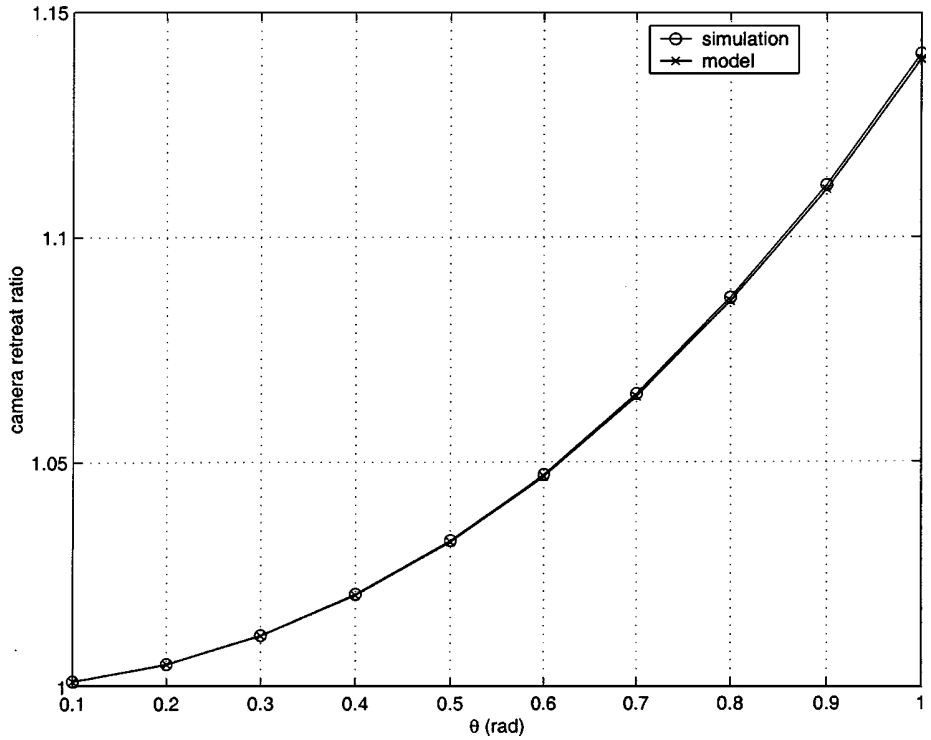

Fig. 4. Comparison of camera retreat ratios observed in simulation and from [7].

nonunique solutions must be dealt with. This method is computationally complex, though tractable in real-time and requires coplanar feature points. We now describe our new approach, which does not exploit the epipolar geometry of the desired and initial images and does not use any explicit 3-D information.

V. A New Partitioned IBVS Scheme

Our approach [14] is based on the observation that, while IBVS works well for small motions, problems arise with large motions and particularly those involving rotation about the z axis. Our proposed partitioned scheme singles out just Z-axis translation and rotation for special treatment, unlike the hybrid approaches mentioned above which treat all three rotational degrees of freedom specially. The motivation for the new partitioning is that camera retreat is a Z-axis translation phenomenon and IBVS failure is a Z-axis rotation phenomenon.

We partition the classical IBVS of (1) so that

$$\dot{f} = J_{xy}\dot{r}_{xy} + J_z\dot{r}_z \tag{9}$$

where $\dot{r}_{xy} = [Tx\ Ty\ \omega_x\ \omega_y]$, $\dot{r}_z = [T_z\ \omega_z]$ and J_{xy} and J_z are, respectively, columns $\{1, 2, 4, 5\}$ and $\{3, 6\}$ of J. Since $\dot{r}_z$ will be computed separately, we can write (9) as

$$\dot{r}_{xy} = J_{xy}^{+}\left\{\dot{f} - J_z\dot{r}_z\right\} \tag{10}$$

where $\dot{f}$ is the feature point coordinate error as in the traditional IBVS scheme.

The Z-axis velocity, $\dot{r}_z$, is based directly on two new image features that are simple and computationally inexpensive to compute. The first image feature, $0 \leq \theta_{ij} < 2\pi$, is the angle between the u axis of the image plane and the directed line segment joining feature points i and j. This is illustrated in Fig. 5. For numerical conditioning, it is advantageous to select the longest line segment that can be constructed from the feature points and allowing that this may change during the motion as the feature point configuration changes. The rotational rate is simply

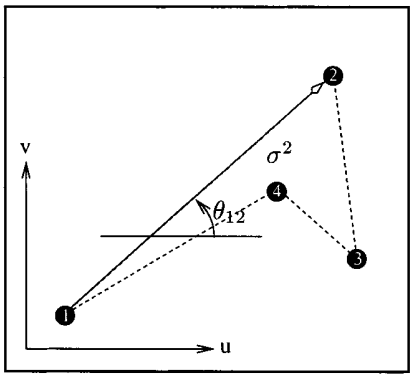

Fig. 5. Image features for new partitioned IBVS control.

$$\omega_z = \gamma_{\omega_z}(\theta_{ij}^{*} - \theta_{ij})$$

in which γ_{ω_z} is a scalar gain coefficient. This form allows explicit control over the direction of rotation, which may be important to avoid mechanical motion limits.

The second new image feature that we use is a function of the area of the regular polygon whose vertices are the image feature points (see Fig. 5). The advantages of this measure are that: 1) it is a scalar; 2) it is rotation invariant thus decoupling camera rotation from Z-axis translation; and 3) it can be cheaply computed (e.g., using the method of Wilf and Cunningham [15]). The feature that we choose to use is the square root of area

$$\sigma = \sqrt{\text{area}}$$

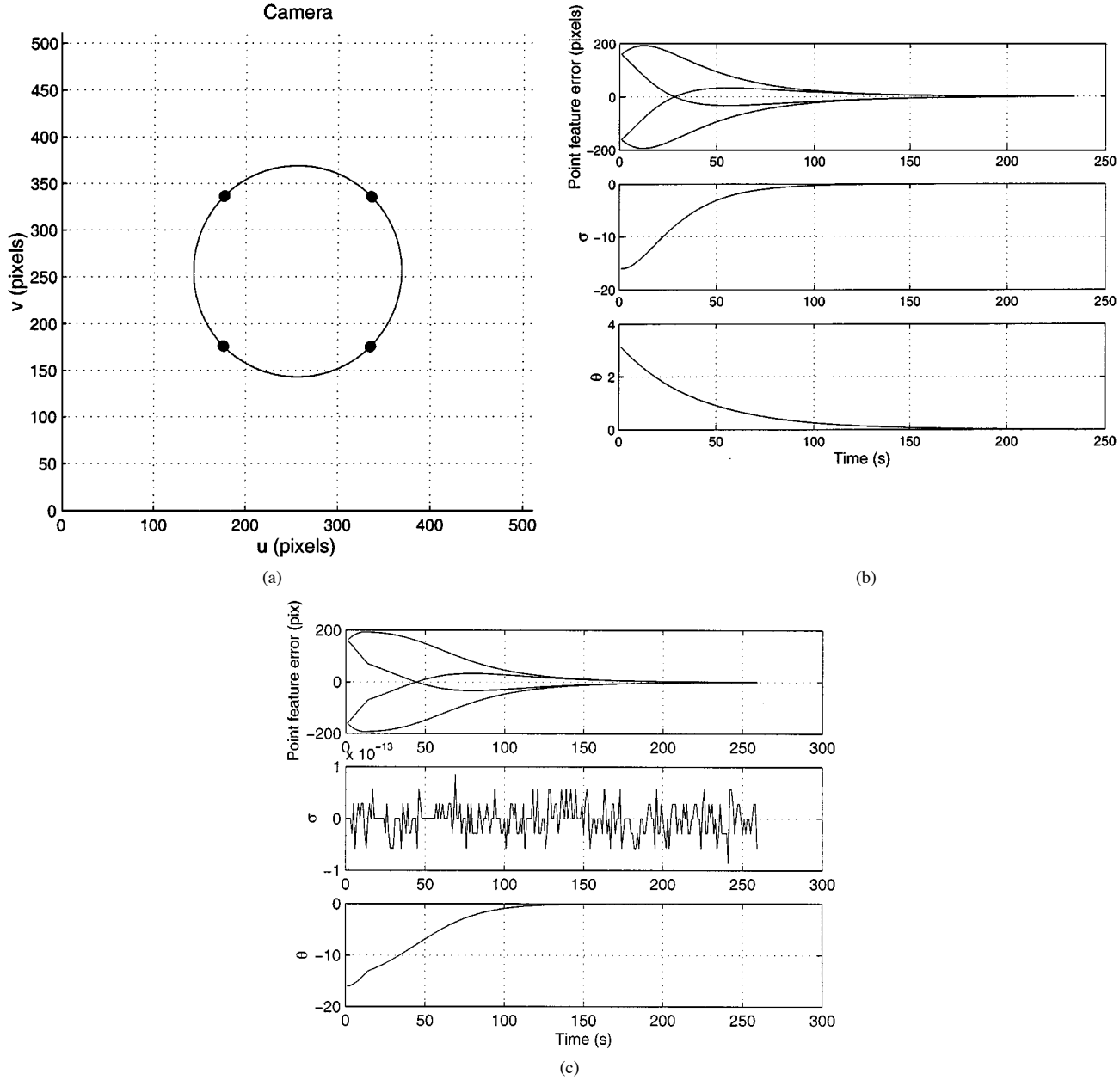

Fig. 6. Proposed partitioned IBVS for pure target rotation (π rad). (a) Image-plane feature motion (initial and desired location are overlaid •). (b) Feature error trajectory. (c) Cartesian translation trajectory.

which has the dimension of length, giving this feature the units of pixels and thus a similar magnitude control gain as for the features $\dot{f}$. The camera z-axis translation rate is thus given by

$$T_z = \gamma_{T_z}(\sigma^* - \sigma). \tag{11}$$

where γ_{ω_z} is a scalar gain coefficient.

Fig. 6 shows the performance of the proposed partitioned controller for the Chaumette Conundrum. The important features are that the camera does not retreat since $\sigma^* = \sigma$. The rotation θ monotonically decreases and the feature points move in a circle. The point feature coordinate error is initially increasing, unlike the classical IBVS case in which feature error is monotonically decreasing. For pure rotation, the point feature error must increase before it can decrease. Note also that the Cartesian translational motion [see Fig. 6(c)] is essentially zero.

An example that involves more complex translational and rotational motion is shown in Fig. 7. The new features decrease monotonically, but the error in f does not decrease monotonically and the points follow complex curves on the image plane.

Fig. 8 compares the Cartesian camera motion for the two IBVS methods. The proposed partitioned method has eliminated the camera retreat and also exhibits better behavior for the X- and Y-axis motion. However the consequence is much more complex image plane feature motion that admits the possibility of the points leaving the field of view, a topic which will be discussed in Section VI.

The features discussed above for z-axis translation and rotation control are simple and inexpensive to compute, but work best when the target normal is within $\pm 40^\circ$ of the camera's optical axis. When the target plane is not orthogonal to the optical axis its area will appear diminished, due to perspective, which causes the camera to initially approach the target. Perspective will also change the perceived angle of a line segment which can cause small, but unneccessary, z-axis rotational motion. Other image features can however be used within this

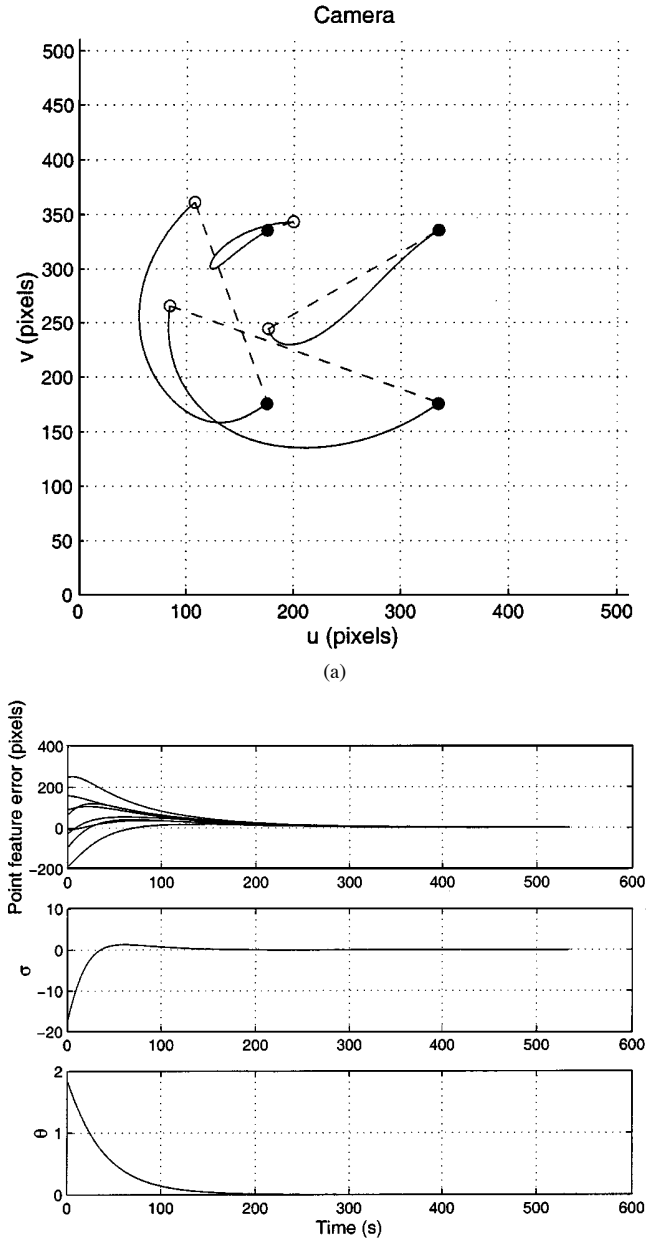

(a)

(b)

Fig. 7. Proposed partitioned IBVS for general target motion. (a) Image-plane feature motion (dashed line shows straight line motion for classical IBVS) and (b) Feature error trajectory.

partitioning framework. The ability to explicitly control z-axis translational motion is of particular benefit for controlling the field of view, as will be discussed in the next section.

VI. Keeping Features in the Image Plane

In order to keep all feature points inside the viewable portion of the image plane at all times, we borrow collision avoidance techniques from the robot motion planning community. In particular, we establish a repulsive potential at the boundary of the viewable portion of the image and incorporate the gradient of this potential into the control law. We use the simple potential given by

$$U_{\text{rep}}(u,v) = \begin{cases} \frac{1}{2}\eta\left(\frac{1}{\rho(u,v)} - \frac{1}{\rho_0}\right) & : \quad \rho(u,v) \le \rho_0 \\ 0 & : \quad \rho(u,v) > \rho_0 \end{cases} \tag{12}$$

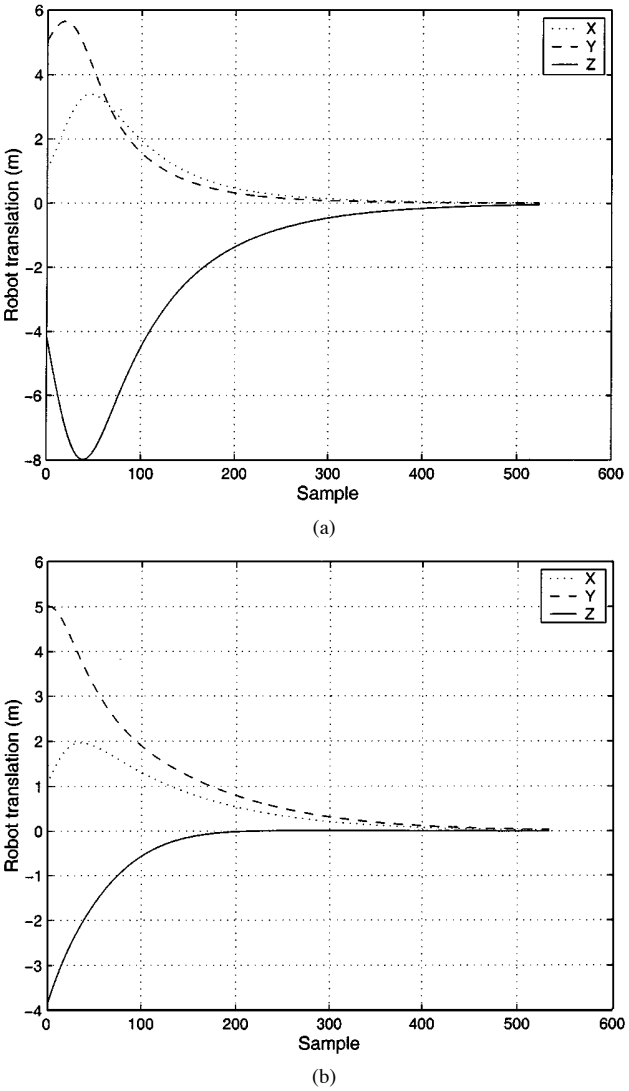

(a)

(b)

Fig. 8. Comparison of Cartesian camera motion for classic and new partitioned IBVS for general target motion.

in which $\rho(u,v)$ is the shortest distance to the edge of the image plane from the image point with coordinates (u,v). The value ρ_0 specifies the zone of the image in which U_{rep} affects the control; if the feature point is not within distance ρ_0 of the boundary, then the corresponding motion is not affected by U_{rep}. The value of η is a scalar gain coefficient.

For an $N_r \times N_c$ image, the value of ρ is easily computed as

$$\rho(u,v) = \min\{u, v, N_r - u, N_c - v\}. \tag{13}$$

If $\mathbf{n}$ is the unit vector directed from the nearest boundary to image feature point with coordinates (u,v), then $\nabla U_{\text{rep}} = F\mathbf{n}$, with F given by

$$F(u,v) = \begin{cases} \eta\left(\frac{1}{\rho(u,v)} - \frac{1}{\rho_0}\right)\frac{1}{\rho^2(u,v)} & : \quad \rho(u,v) \le \rho_0 \\ 0 & : \quad \rho(u,v) > \rho_0 \end{cases}. \tag{14}$$

Since a pure translation in the negative z direction will cause feature points to move toward the center of the image, the value of F is mapped directly to the T_z component of the velocity command by combining it with the control given in (11). In a discrete-time system, we observe a chatter phenomenom (where the feature points oscillate in and out of

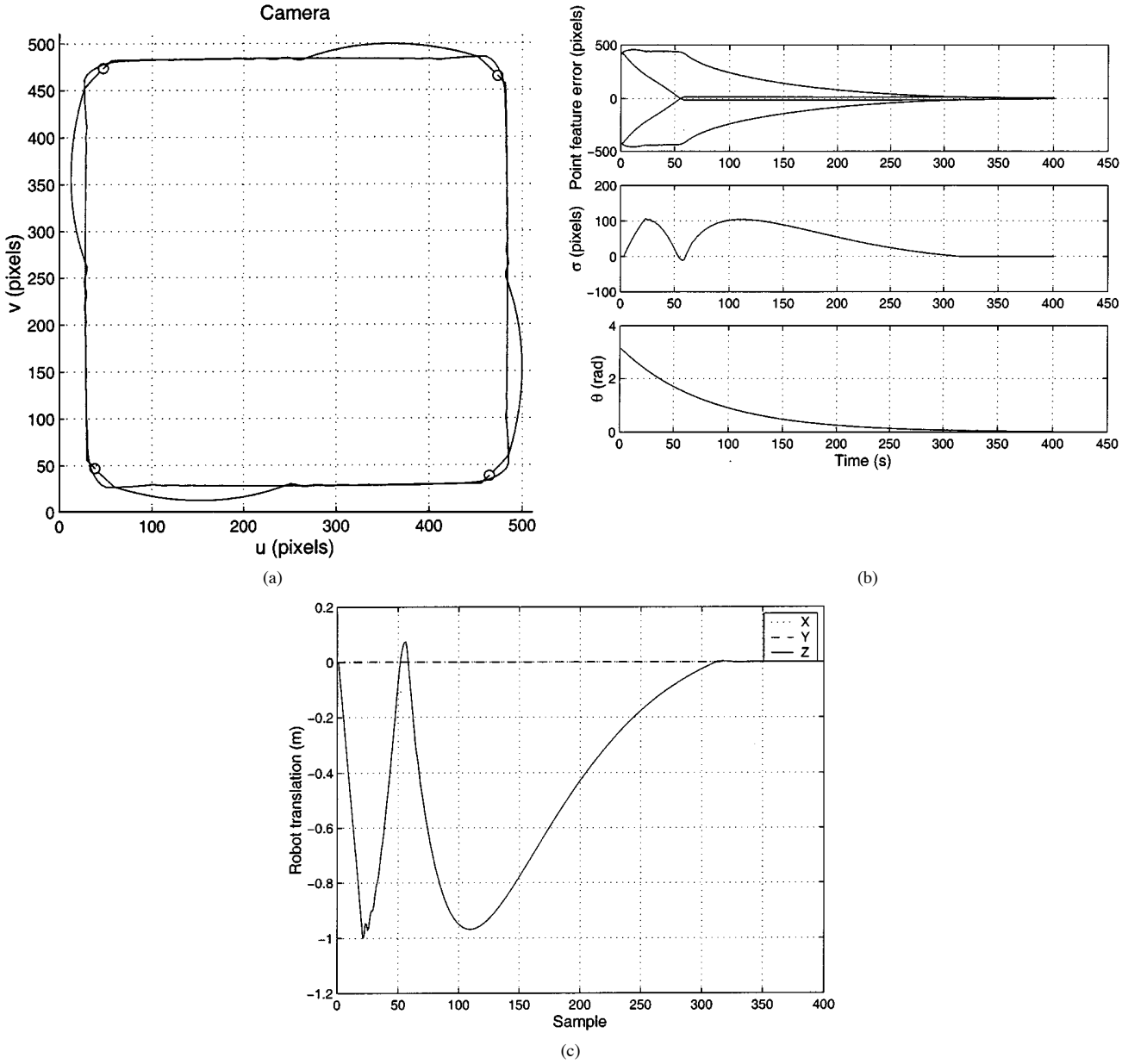

Fig. 9. Proposed partitioned IBVS with collision avoidance for pure target rotation (π rad). (a) Image-plane feature motion (initial location is o, desired location is •). (b) Feature error trajectory. (c) Cartesian translation trajectory.

the potential field); we smooth and clip the resulting T_z, yielding the discrete-time controller

$$T_z'(k) = \mu T_z'(k-1) + (1-\mu)(\sigma^* - \sigma - F) \tag{15}$$

$$T_z = \min\left\{\max\left\{T_z'(k), T_{z_{\min}}\right\}, T_{z_{\max}}\right\}. \tag{16}$$

In simulation, we found it advantageous to use asymmetric velocity clipping where $|T_{z_{\max}}| < |T_{z_{min}}|$, that is, the camera can retreat faster than it can approach the target. This reduces the magnitude of the "bounces" off the boundaries of the image plane when points first enter the potential field. In practice, this smoothing and clipping may not need to be explicitly implemented, since any real robot will have finite bandwidth and velocity capability.

The use of a potential field raises the issue of local minima in the field, but in our case, these issues do not arise. The potential field is used merely to force a camera retreat and since it will be possible for the system to achieve the goal when this retreat is effected (in this case, we merely approach the performance of the classical IBVS system). Of course, this assumes that no goal feature point locations lie within the influence of the potential field. A similar use of potential fields is given in [16].

Results of the new partitioned IBVS with collision avoidance are shown in Fig. 9. The target is larger than before, so that as the camera rotates the feature points move into the potential field. The parameters used were $\eta = 5\times10^6$ and $\mu = 0.8$. It can be seen that as the points are rotated, they move into the potential field and then follow a path parallel to the edge, where the boundary repulsion and target area components of the T_z demand are in equilibrium.

For high rotational rates, the chatter phenomenon will occur and at very high rates the points may pass through the potential field and become trapped *outside* the image plane. Rotational rate should properly

be controlled by another loop, and this problem has strong similarities to that of controlling step size in numerical optimization procedures.

VII. Conclusion

In this paper, we have investigated some problems with classical image-based visual servoing and proposed a new partitioned visual servoing scheme that inexpensively overcomes these limitations. We have also provided simple geometric insight into the root cause of the undesirable camera retreat phenomenon and the pathological case we have termed IBVS failure.

Other hybrid IBVS schemes have been recently proposed and are based on decoupling camera translational and rotational degrees of freedom. We have proposed a different decoupling and servo Z-axis rotation and translation using decoupled controllers based on two easily computed image features.

All hybrid schemes admit the possibility of points leaving the image plane, as does the approach that we described in Section V. In this paper, we considered this to be a collision avoidance problem and employed potential field techniques to repel the feature points from the image boundary.

References

[1] A. C. Sanderson, L. E. Weiss, and C. P. Neuman, "Dynamic sensor-based control of robots with visual feedback," *IEEE Trans. Robot. Automat.*, vol. RA-3, pp. 404–417, Oct. 1987.

[2] J. Feddema and O. Mitchell, "Vision-guided servoing with feature-based trajectory generation," *IEEE Trans. Robot. Automat.*, vol. 5, pp. 691–700, Oct. 1989.

[3] D. B. Westmore and W. J. Wilson, "Direct dynamic control of a robot using an end-point mounted camera and Kalman filter position estimation," in *Proc. IEEE Int. Conf. Robot. Automat.*, 1991, pp. 2376–2384.

[4] F. Chaumette, "Potential problems of stability and convergence in image-based and position-based visual servoing," in *The Confluence of Vision and Control*, D. Kriegman, G. Hager, and S. Morse, Eds. Berlin, Germany: Springer-Verlag, 1998, vol. 237, pp. 66–78.

[5] E. Malis, F. Chaumette, and S. Boudet, "2-1/2-d visual servoing," *IEEE Trans. Robot. Automat.*, vol. 15, pp. 238–250, Apr. 1999.

[6] G. Morel, T. Liebezeit, J. Szewczyk, S. Boudet, and J. Pot, "Explicit incorporation of 2d constraints in vision based control of robot manipulators," in *Experimental Robotics VI*, P. Corke and J. Trevelyan, Eds. Berlin, Germany: Springer-Verlag, 2000, vol. 250, pp. 99–108.

[7] K. Deguchi, "Optimal motion control for image-based visual servoing by decoupling translation and rotation," in *Proc. Int. Conf. Intelligent Robots and Systems*, Oct. 1998, pp. 705–711.

[8] S. Hutchinson, G. Hager, and P. Corke, "A tutorial on visual servo control," *IEEE Trans. Robot. Automat.*, vol. 12, pp. 651–670, Oct. 1996.

[9] B. Espiau, F. Chaumette, and P. Rives, "A new approach to visual servoing in robotics," *IEEE Trans. Robot. Automat.*, vol. 8, pp. 313–326, 1992.

[10] K. Hashimoto, T. Kimoto, T. Ebine, and H. Kimura, "Manipulator control with image-based visual servo," in *Proc. IEEE Int. Conf. Robotics and Automation*, 1991, pp. 2267–2272.

[11] N. P. Papanikolopoulos, P. K. Khosla, and T. Kanade, "Visual tracking of a moving target by a camera mounted on a robot: A combination of vision and control," *IEEE Trans. Robot. Automat.*, vol. 9, pp. 14–35, Feb. 1993.

[12] P. Oh and P. Allen, "Visual servoing by partioning degrees-of-freedom," *IEEE Trans. Robot. Automat.*, vol. 17, pp. 1–17, Feb. 2001.

[13] O. Faugeras, *Three-Dimensional Computer Vision*. Cambridge, MA: MIT Press, 1993.

[14] P. I. Corke and S. A. Hutchinson, "A new partitioned approach to image-based visual servo control a new partitioned approach to image-based visual servo control," in *Proc. 31st Int. Symp. Robot.*, Montreal, May 2000, pp. 30–35.

[15] J. Wilf and R. Cunningham, "Computing Region Moments From Boundary Representations," NASA JPL, JPL 79–45, 1979.

[16] Y. Mezouar and F. Chaumette, "Path planning in image space for robust visual servoing," in *Proc. IEEE Int. Conf. Robot. Automat.*, San Francisco, Apr. 2000, pp. 2759–2764.

Computation of 3-D Form-Closure Grasps

Dan Ding, Yun-Hui Liu, and Shuguo Wang

***Abstract*—In this paper, we address the problems of computing form-closure regions as well as computing optimal fingertip locations yielding n-finger form-closure grasps of three-dimensional (3-D) objects. Given grip points of k fingers not in form-closure, we propose a sufficient and necessary condition for the $n - k$ fingers to achieve a n-finger form-closure grasp. Based on the condition, it is demonstrated that the problem of computing form-closure regions can be formulated as an existence problem of a solution for a set of inequalities. A sufficient condition is also proposed to simplify the computation of form-closure regions. As to searching for optimal fingertip locations, we transform the problem to a nonlinear programming problem subject to a set of constraints arising from that sufficient and necessary condition. Furthermore, a performance index is defined by measuring the distance between the center of mass of the grasped object and the center of the contact points. Finally, we have implemented the approach proposed and verified its efficiency by several numerical examples.**

***Index Terms*—Form-closure grasps, multifingered robot hand, nonlinear programming, optimal grasp planning.**

I. Introduction

In recent years, there has been a growing interest toward a multifingered robot hand due to its flexibility and dexterity. Works related to multifingered grasping involve mechanical design [18], stability analysis [1], kinematics [3], and dextrous manipulation [17].

The stability of a grasp is one of the fundamental issues concerning multifingered grasping, the subject therefore attracted much attention over the last decade. The stability of multifingered grasping is characterized by form-closure or force-closure [1], [12] property under which arbitrary forces and torques exerted on the grasped object can be balanced by the contact forces applied by the fingers. In other words, the finger placements for a form-closure grasp should be that whenever the directions or magnitudes of the applied contact forces are changed, the robot hand can still keep the object grasped without being disturbed by any external force/torque that might otherwise cause the object to slide or rotate. In this sense, the computation of fingertip positions ensuring form-closure property constitutes an essential problem. Salisbury and Roth [12] have demonstrated that a necessary and sufficient condition for form-closure is that the primitive contact wrenches resulted by the contact forces positively span the entire wrench space. This condition is equivalent to that the origin of the wrench space lies strictly inside the convex hull of the primitive contact wrenches [8], [20].

A general survey on grasp synthesis can be found in [19]. Research efforts toward the stability of a grasp have been directed to testing and synthesis problems. Works related to testing form-closure property of a given grasp can be found in [4], [7], [13]. Literatures related to two-dimensional (2-D) grasp synthesis are available in [5], [9], [10]. However, only a few works touched the topic of computing three–dimensional (3-D) form-closure grasps due to the complicated

Manuscript received August 17, 2000; revised April 2, 2001. This paper was recommended for publication by Associate Editor J. Ponce and Editor A. De Luca upon evaluation of the reviewers' comments. This work was supported in part by the Hong Kong Research Grant Council under Grant CUHK 4151/97E, Grant CUHK 4166/98E, and Grant CUHK 4217/01E.

D. Ding and Y.-H. Liu are with the Department of Automation and Computer-Aided Engineering, Chinese University of Hong Kong, Hong Kong, China (e-mail: dding@mae.cuhk.edu.hk; yhliu@mae.cuhk.edu.hk).

S. Wang is with the Robotics Institute, Harbin Institute of Technology, Harbin, China (e-mail: sgwang01@robinst.hit.edu.cn).

Publisher Item Identifier S 1042-296X(01)07461-4.